Cancer detection using deep learning techniques

[1]SADANANDA PATTANAYAK,
Gandhi Institute of Excellent Technocrats, Bhubaneswar, India
[2]SUBHAM SAMANTARAY,
Aryan Institute of Engineering & Technology, Bhubaneswar, Odisha, India

Abstract

Breast cancer has become the most common form of cancer in world recently having overtaken cervical cancer in urban cities. Immense research has been carried out on breast cancer and several automated machines for detection have been formed, however, they are far from perfection and medical assessments need more reliable services. Computer Assisted Diagnostics programs have been developed over the past 2 decades to help radiologists interpret mammogram screening. Deep convolutional neural networks (CNN), which have surpassed human output since 2012, have been an immense suc- cess in image recognition. Deep CNNs will revolutionize the analysis of medical images. We propose a method for breast cancer detection based on Faster R-CNN, the most common frameworks for object detection. In a non-human interference mammogram, the device detects and categorizes malignant or benign lesions. The method proposed sets the current status of the INbreast database public classification scheme, AUC = 0.95. In the digital mammography challenge DREAM with AUC = 0.85, the method mentioned here was second. When the device is used as a sensor, the accuracy of the INbreast data set is extremely low with very false positive image points.

Keywords Convolutional neural networks · Deep learning · Mammography · Breast cancer screening · Breast density

1 Introduction

Breast cancer is the leading cause of women and worldwide breast cancer death [1]. Mammography screening has shown a 38–48% decreasing death rate among participants of breast cancer [2]. In 25 out of the 27 Member States of the EU, initiatives for the detection and treatment of breast cancer are under preparation, piloting or introducing screenings [3]. X-ray pictures are taken from two sides of each breast during normal mammographic screening. One or two specialized radiologists examine these images for malignant lesions'. For further diagnostic evaluation suspected cases are demanded. Human readers test screening mammograms. The reading method is one-size-fits-all, tiring, Lengthy, costly and mostly mistaken. Several reports have shown that the previous negative screening test by blinded reviewers retrospectively shows 20–30% of cancer diagnoses [4]. Despite the latest FFDM [4, 5], the issue of lack of cancer remains a matter of full digital mammography. The responsiveness and the unique characteristics of screening.

Mammograms are 77–87% and 89–97%. These statistics reflect readers 'average performance and there are significant differences in individual doctors' results, with recorded false positive levels of 1–29% and sensitivities of 29–97%. The output was improved by double reading and introduced in several countries. Double reading was found. More than 10 readers will boost their diagnostic efficiency and show that mammograms have room for development beyond duplication. The rapid growth of machine learning and in particular profound Expertise continues to drive the healthcare industry's interest in applying these technologies to boost the precision of cancer screening. Mammograms have been found to minimize mortality [7] and American women suffer from breast cancer as the second leading cause

of death [6]. Despite its advantages, screening mammograms are extremely likely to produce false positive and false negative tests [8]. The average sensitivity of mammography for optical screens is 84.4% and the overall specificity is 90.8%, according to a report carried out in 2009 by the Breast Cancer Surveillance Consortium (BCPC). Computer-assisted diagnostic detection (CAD) software (as revised in [9]) the radiologists' predictive accuracy in testing mammography was improved and in clinical use since the 1990s. Sadly, there is evidence that commercial CAD systems have not brought about substantial changes in performance [10], and growth has stagnated over the last ten years. With its remarkable success in in-depth learning in the identification and detection of visual artifacts, it is important to help radiologists and enhance screening accuracy in many other areas [11, 12].

The early detection of subclinical breast cancer as an image recognition task is difficult, as the tumors themselves occupy only a very small part of the breast picture. A full-field FFDM image, for example, usually shows 4000 per 3000 pixels while a ROI can be just as small as 100 to 100 pixels. If mammography database ROI annotations are regularly available, the object detection and classification procedures could be easily implemented, for example, the regional R-CNN [13] and the regionally-based neuronal convolutional network [13]. However, ROI annotations [14] approaches are often not large-transferable; expensive mammograms that lack ROI annotations. In addition, there are few public repositories of mammography [15] annotated. However, in-depth education needs the most powerful broad data sets. Only the few completely annotated datasets and large datasets with a cancer status for each picture will boost the accuracy of brain cancer classification algorithms. Pre-training is a safe way of approaching the issue of preparation. Hinton et al. [16] for example used pre-training in the layer in order to initialize the deep belief (DBN) weight parameters with the three secret layer and then to fine-tune them in order to identify them. They noticed the training pace and the accuracy of handwritten visual recognition improved before the class. Firstly, a deeper learning models for an extensive database such as ImageNet are developed and finalized [17]. Since the new function is not linked to the initial training data collection, the weight parameters of the model are already initialed and can easily be used for a different job to identify fundamental features such as borders, corner and textures. Additionally, time saved and machine performance increased [19].

A variety of approaches for object detection with deep learning is included in the computer vision literature. The region-based convolutional networks (RCNNs) seek to gather bordering the targets boxes with position and target sizes information. RCNN is sadly incredibly sluggish and expensive in computing. For that reason, the faster and more effective RCNN [20, 21] was constructed on the basis of a complete, joint training program Both the national CNN initiatives and the weight-sharing national classification module. This improves the sensitivity and speed of the RCNN to objects in comparison with RCNN or RCNN with these characteristics. However, it does lack literature on how this system could be used for mass sensing in DBT, thus reducing time-consuming properties. We analyzed how easily the R-CNN can be used to screen for ROIs and the difference between real masses and FPs in DBT. We compared its findings on the public INbreast database, AUC = 0.95. The proposed method sets the state-of-the-art classification performance on the public INbreast database, AUC = 0.95. The approach described here has achieved the 2nd place in the Digital Mammography DREAM Challenge with AUC = 0.85. When used as a detector, the system reaches high sensitivity with very few false positive marks per image on the INbreast dataset. When used as a detector, this device is very sensitive with very few false positive characteristics per picture in the INbreast dataset.

2 Proposed system

The proposed method employs Faster RCNN object detection framework to classify and localize breast cancer lesions as benign or malignant. Faster R-CNN is the core of our model and focuses on a convolutional network for the detection and placement of objects in an image, with additional components. Quick R-CNN has a division called the Area Network Proposal, which identifies and localizes objects within the image regardless of the object size, after the last convolutional layer of the original network. Automatic screens of various dimensions and aspect ratios are required to find items of different sizes and shapes. The area proposals for the other sector of the network are considered the top scoring default boxes. The other neural network branch measures the signal from each area that is measured at a fixed size of the last convolutional layer. To improve the boundaries of the object in the sector, both branches attempt to resolve the classification challenge and the bounding regression challenge. The best predictions can be selected using non-maximum deletion from the detected overlapping objects. The initial article provides more detail on Faster R-CNN. Figure 1 display a pattern outline. Distribution of value (excluding background) and re-scaling to 0–255. A 16-layer deep VGG16 network was the basis for our plan. Two kinds of images, milder lesions or malignant lesions can be identified by the final layer. For each lesion found, the model generates a bounding box and a result that represents trust in the lesion class. In order to define a single scoring picture, we use the maximum scores of all malignant lesions found for several and we take the average number of photos

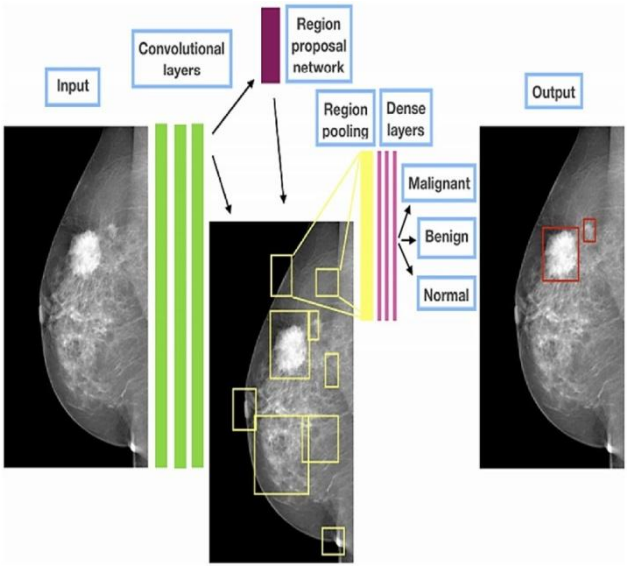

Fig. 1 The outline of the Faster R-CNN model for CAD in mammography

of the same breast. Two models with shuffled training data sets have been created for the DM challenge. The picture score for the assembly of those models was the average score of each model. An earlier research on autonomous yet quick and functional human readers has influenced this approach. It's been very good. The Faster R-CNN [18] Framework was developed by the developers, which was integrated into the Caffe deep learning framework. The proposed CAD have optimized during training the object detection aspect and the model rating component. We used back propagation and stochastic decrease in weight of gradients. The first trained model with ImageNet images was 1, 2 million.

Higher resolution performs better, because mammograms are isotropically rescaled on the shorter side, a longer side of less than 2100 pixels or under 1700 pixels. This resolution is similar to the full graphics card memory. In line with the Hologic norm aspect ratio, the dimension ratio has been chosen.

In order to increase the training dataset, the proposed CAD used vertical and horizontal rotation. Mammograms contain fewer artifacts than usual images, thus mini-batches dominate negative propositions. In order to allow more positive measurements in each mini-batch it has been reduced from 0.7 to 0.5 the threes for front-end artifacts in the area Proposed Network intersection over Union (IoU). It also relieves positive evidence that mammalian lesions are much less defined than in a typical photograph of a car or dog. The final, non-maximum (nms) deletion IoU threshold was set at 0.1, despite the fact that mammograms reflect a smaller and more compact 3D space compare to ordinary pictures. The model was trained for 40 k iterations. The previous testing of the DM challenge training data showed that this amount is close to optimal.

In this work, Faster R-CNN CAD method is suggested, reaching 2nd in the AUC range = 0.95 in the Digital Mammography Challenge final validation results. The findings of the competition have proved to be one of the best methods to classification of mammograms for cancer. The DM problem concentrated on recognizing malignant lesions and the picture.

Classification as a whole was the only method that the proposed system used to get away from the identification mission. An accident detector is much safer clinically than a listen. Just one single marker may be given for a case or breast, but the cancer that is necessary for additional diagnosis or treatment is unable to be identified.

Data sets

The model was based on a public mammography screening (DDSM) digital database and an INbreast public data collection data set from the University of Semmelweis in Budapest. The photos used for the training contain histologically confirmed cancers or stable injuries, reminiscent of which were not malignant after further testing. Our understanding with both lesions is anticipated to help our model recognize more lesions and to distinguish between malignant and benign examples.

The INbreast dataset comprises 115 FFDM cases of ground-level pixel realities and histological evidence for cancer. In conjunction with our test scenario the INbreast pixel annotations have been modified. The benign annotations were overlooked and the malignant lesion annotations were translated into bounding boxes. Eight studies with additional observations, objects, past procedures, or unclear disease outcomes were omitted. Thus we have changed the pixel level range, with the images of low contrast. The pixel values have been cut to 500 pixels less and 800 pixels higher than the pixel mode.

DDSM includes more than 2620 scanned mammograms, including mild, Pathological details reviewed in benign and malignant cases (see Fig. 2). For the case of a single craniocaudally bilateral (CC) and an oblique Medio lateral (MLO), four mammograms with two separate views are observed. In benign and malignant cases, important abnormality information is provided.

Image preprocessing

The 3D bounding box was annotated manually by an experienced radiologist and the ROIs extracted from the precise positions of the radiologist, the true mass of TP groups. The screening ROIs represented the FP artefacts. The Fig. 3

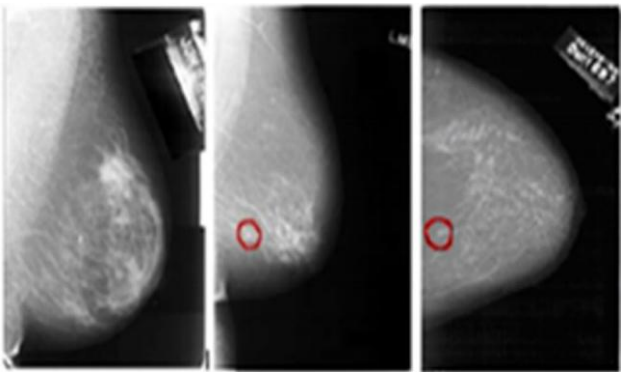

Fig. 2 Taking DDSM mammograms. From left to right: breast without any evidence of abnormality, tumor breast and benign tumor breast

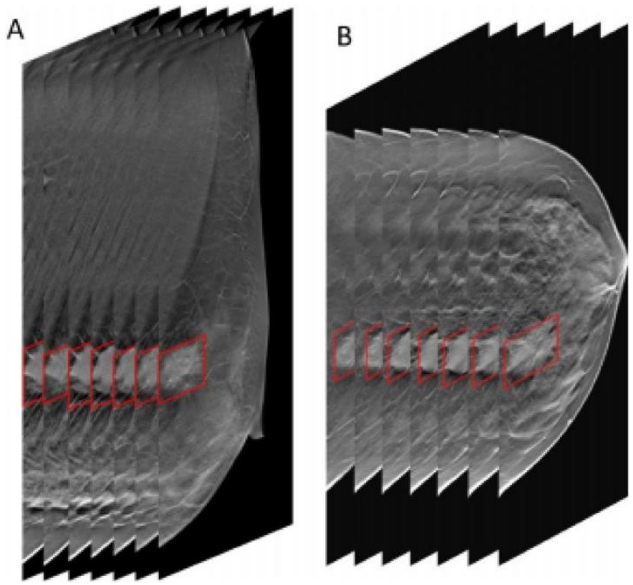

Fig. 3 An example of the mass ROI annotation in **a** MLO and **b** CC images for DBT images

displays a manual mass annotation in two views of different sizes on DBT images.

Since the acquired in-plane resolution (including 49.5 to 49.5 μm) from Siemens is comparatively bigger than that of UIS, all UIS sliced images are sampled in an in-plane resolution of 85 μm to be able to achieve an equivalent resolution of 85–85 μm using a bi-cubic interpolation algorithm [22]. A 3D Laplacian filter of 3 × 3x3 was used in all volumes of DBT to boost the edges of the tumor. In addition, a two-view (CC and MLO views) knowledge fusion approach was used to classify the automatic nipple location [23]. Afterwards, the skin and context were omitted from the breast region using a complex multiple thresher dependent breast boundary method, as shown in the Fig. 4 [24, 25]. This picture

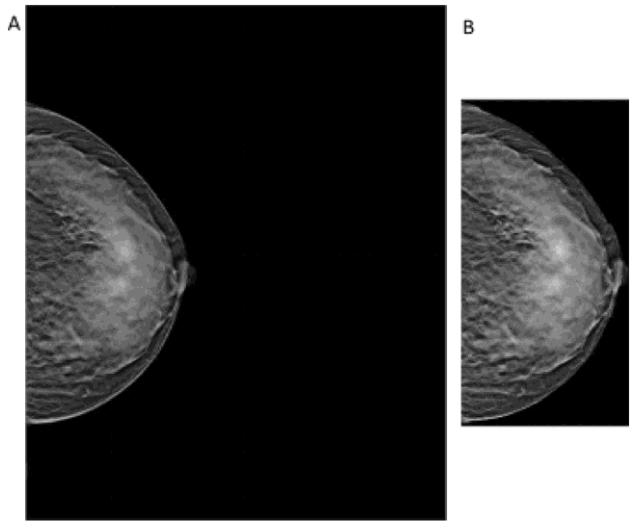

Fig. 4 An example of the removal of the skin. **a** First, broad-based slice. **b** Surface and skin preprocessed image removed

preprocessing was performed to prevent large scale measurements of RCNN CAM background pixels.

3 RCNN-based CAD

In this section, the structure and specification for the faster RCNN model were briefly presented in our RCNN CAD framework.

Faster RCNN architecture and hyper parameters

The Faster R-CNN model was updated using 5 coated layers in the previous study in our RCNN CAD framework [26], using DCNN architectural features. As Fig. 5 shows. The RCN Network Fig. 5a consists of two major constituents for the faster RCNN model: (1) a Regional Proposition Network (RPN), a profoundly convolutional network that produces proposal bounded boxes in an input picture with all sizes. In addition, each projected bounding box and convolution features in the ROI pooling layer are accepted. To obtain information about the TP likelihood and location, a SoftMax layer and bounding box regression are used. In the single network, RPN and Classifier networks shared a broad image convergence, which reduced the time required to produce regional propositions dramatically. As shown in Fig. 5b, the network consists of 5 standard coagulation layers (C1, C2, C3, C4, C5) and 2 total coagulation layers between C1 and C2, C2 and C3 Fig. 5b. The typical convolutional layers are 96, 128, 384, 192 and 128 filter kernel sizes, respectively, of 11 × 11, 5 × 5, 3 × 3, 3 × 3 and 3 × 3, respectively. The unique convolutional layers (C6, C7, and C8) of RPN have 256, 14, and 28 filter kernels of sizes of 3 × 3, 1 × 1, and 1 × 1,

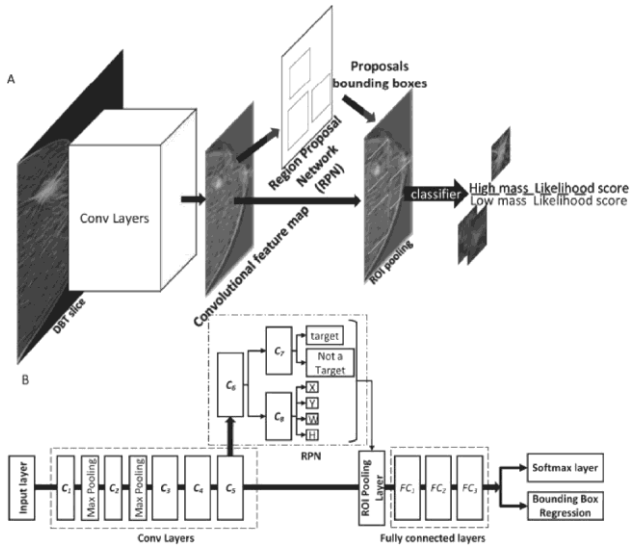

Fig. 5 Our faster RCNN-based CAD device platform and architecture. **a** Fast RCNN mass detection framework in DBT pictures. **b** Faster RCNN-based cad architecture

respectively. The network of classifiers contains three fully-connected layers (FC1, FC2 and FC3) with 4096, 4096 and two neurons. Anchor boxes with various dimensions and aspect ratios were used for detecting masses with different sizes on each sliding window on a convolution diagram. Six scales (1, 0.5, and 2), have been used for each anchor, which produced 18 anchors at a sliding window location. Three scales (182, 372, 722, 1442, 2882, have been employed and 5762 pixels). The previous research offers thorough explanations of this method [27].

The heat-map is flattened and connected to the image classification output by means of FC layers in a simple approach to creating a whole image classifier from a patch classifier. A maximum pooling layer after the heat-map is necessary to improve the translational invariance of the model to the performance of the patch classifier. In addition, the heating map and the output can be simplified to simplify preparation. The heat-map is from the output of the patch classifier, which is activated by the softmax:

$$f(z)_j = \frac{e^{z_j}}{\sum_{j=1}^{e} e^{z_i}} \quad for\ j = 1, \cdots, C \tag{1}$$

The Softmax activation however reduces gradients for large inputs which, in an intermediate layer, can impede gradient flow. Consequently, linear corrected units (ReLU) can instead be used:

$$f(z)_j = \max\ 0, z_j \quad for\ j = 1, \cdots, C \tag{2}$$

The activation is always supported to be ReLU unless otherwise specified when referring to the heat map in a whole image classifier.

Faster RCNN training

For faster RCNN preparation, sampling from a Gaussian distribution randomly initialized all weights. The initial 0.001 learning rate was used for all layers experimentally. For every 20 epochs there was a stepwise procedure for raising the learning rate by 0.1. In learning kernels, an L2 control concept was used to minimize overfitting for the weights of loss functions. A method was also used to randomly drop a node in a hidden layer and a chance was calculated to drop all the hidden node values to 0.5. A four-stage algorithm with alternating optimization was used to learn network parameters for training faster RCNN. The RPN have been trained for the first time as a candidate mass in Phase 1 with the initialized network. In Step 2, a different classification network was trained using the RPN boxes in Step 1. All networks were trained independently at this stage without parameters. Phase 3 was initialized by the qualified Phase 2 network for the purpose of RPN, However, its fundamental learning levels (i.e., C1, C2, C3, C4 and C5) have frozen by 0%. For the second time, the RPN was conditioned by upgrading the different RPN layers (i.e. C6, C7 and C8). Step 4 addresses joint layouts and step 2 redundant for the establishment of the classification scheme, by updating the different RCNN layers more quickly (i.e. FC1, FC2, and FC3).

Here, C7 performance predicts whether the bordering boxes of the proposal reflect a mass. Box center coordinates of C8, i.e. X, Y, W and H, and their width and height, are represented by the C8 outputs. In order to differentiate between the box coordinates, the convolution features and projected bounding systems were transferred to the ROI bond layer. For through proposal bounding, the system produces a mass probability value, size and position information.

4 Result and discussion

In this section the results of the test of the qualified data set images are presented using the python and *MATLAB*© framework. The accuracy was established by the following equation to evaluate the results:

$$Accuracy = 100 \times \frac{TP + TN}{TP + TN + FP + FN} \tag{3}$$

TP means true positives, TN means true negatives, FP means false positives, and FN means false negatives.

If the entire number of images chosen for network training is used as a training input for the training process, the program tested the validation collection. The average accuracy of the classification was 95% in the two groups studied following network formation: benign and malignant tumors the classification.

After these results were collected, the network's output images were analyzed to see the boundary boxes suggested by the machine over their original pictures. The Fig. 6 displays the results of our method for accuracy when tumors inside the dataset samples considered for research are observed. Photos in Fig. 6 left hand is consistent with the output from our method, with border boxes colored in blue, and the correct mark images are shown in the right section, showing where there are tumors, taking this in mind as the ground truth.

Cancer classification

The model efficiency has been also measured with the ROC metric data collection, Fig. 7. The INbreast data collection has many one-hand experiments, so the forecasts have been calculated for each brain. The machine obtained AUC = 0.95, (95 percentile interval from 10,000 bootstrap samples, 0.91 to 0.98). To our knowledge, it is a single model oriented, fully automated device, with the highest AUC in the INbreast dataset.

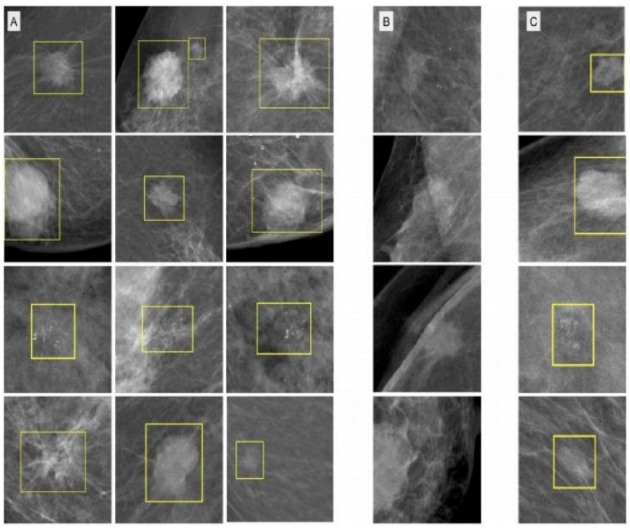

Fig. 6 Examples of detection: The yellow boxes display the model's lesion. The identification threshold was chosen to be 0.9 = lesion sensitivity. **A** Malignant injury, **B** Malignant injury, **C** False positive lesions found correctly

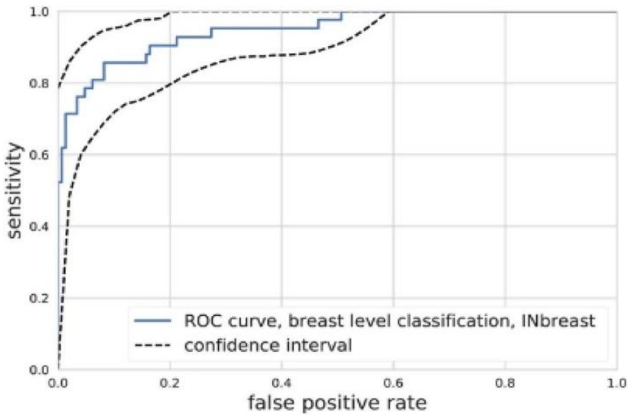

Fig. 7 Classification efficiency. The solid blue line indicates a curve ROC on the breast stage (AUC = 0.95) on the basis of 10,000 bootstrap studies. The dotted lines indicate the 95-percentile curve distribution

FROC analysis

We tested the predictions for the INbreast data set using the free-response ROC (FROC) curve to check the capacity for detecting malignant lesions and locating them accurately. The FROC curve shows sensitivity as the result of the amount of false positive marks inserted in the picture (fraction of correctively localized lesions) as shown in the Fig. 8. The detection was considered correct when the center of the proposed lesion fell within the bottom of a true box.

Generally, the same criteria are used to measure the performance of CAD products currently used. There is no lesion annotation in the DM challenge dataset, so we cannot use it for FROC research.

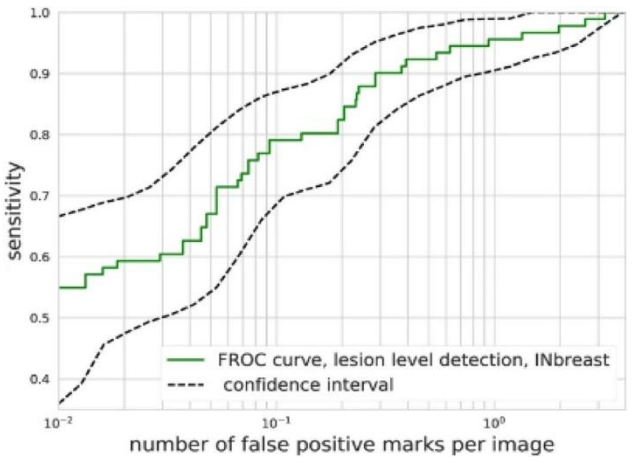

Fig. 8 INbreast dataset's FROC curve. Sensitivity per lesion is determined. The solid curve with squares shows the results with every single image, while the dashed lines indicate the interval of 95 percentiles from 10,000 samples

5 Discussion

We have suggested a Faster R-CNN cad method, reaching 2nd in the AUC range = 0.95 in the Digital Mammography Challenge final validation results. The results of the competition have proven one of the best approaches in cancer mammograms classification. The DM question centered on recognizing malignant injuries while the overall picture classification is an important step away from the task of identification, which was the only method we used. Just one single marker may be given for a case or breast, but the cancer that is necessary for additional diagnosis or treatment is unable to be identified.

We tested the model for the INbreast dataset that was available to the public. In an inbraast dataset, the system detects 90% of damaged injuries with just 0.3 false positives per picture.This also includes the latest data on the public INbreas dataset for cancer ratings. The program only uses mammograms with no annotations and interactions between users.

6 Comparison

We designed and implemented novel algorithms and deep neural networks for pre-processing, visualization and performance enhancement.

- Achieved similar performance on Mass versus Calcification for both models on INbreast, but on AIIMS, FRCNN outperformed Retinanet by missing fewer malignant lesions and correctly identifying more masses and calcifications
- We also tested on small masses wherein both networks gave similar AUC while for localization, FRCNN performed better than Retinanet
- On 20,000 image-labelled AIIMS data, FRCNN gave a higher AUC compared to Retinanet we have built and trained the photometric transform network and are currently testing it and experimenting further by adding hinge loss and modifying hyper parameters (as shown in the Table 1). The Fast R-CNN integrates the region candidate generation, feature extraction and region classification stages in one pipeline. It performs mass detection and segmentation tasks altogether and the network can be optimized as a whole. The proposed CAD does not require massive training of the Faster R-CNN. Each round of training only takes approximately 10 min with 10 epochs. The testing of the Fast R-CNN model takes less than 1 s per image.

Table 1 performance Comparison table

Dataset	FRCNN (proposed)	RetinaNet
INBreast	AUC: 0.95	AUC: 0.941
	Sens: 0.9 at 0.3 FP	Sens: 0.8 at 0.3 FP
DREAM	AUC: 0.85	AUC: 0.805
	Sens: 0.857 at 0.3 FP	Sens: 0.68 at 0.3 FP

In this research four CAD systems' performance have been compared using the FROC area difference [28–30]. The Bootstrap test was used to re-evaluate the output value of the CAD without assuming parameters. The differential distribution was compared to the difference in the metric. The differential was observed. When the measured distribution width was much the discrepancies between methods were found to be significant less than the metric observed. The statistical value of the disparity in output between our CAD systems based on the RCNN, LSTM, DCNN and CNN was determined from the FROC breast curves.

In addition, in the model size, number and time-consuming parameters and AUC, we compared our network with other models. Table 2 shows that the proposed CAD using Faster R-CNN achieves a similar detection performance and a higher segmentation performance compared to [31], and outperforms [32, 33] in both detection and segmentation on INbreast data. Budak et al. [32] and Agarwal et al. [33] both have separate networks for region candidate proposal, classification and mass segmentation, which need to be tuned sequentially, while the proposed CAD integrates all these stages.

Our network obtained a successful outcome with less capacity than DCNN from the contents of Table 2. Although storage space is more than the DCNN, the efficiency and time consuming are significantly better.

7 Conclusion

In this work, we proposed an integrated mammographic CAD for simultaneous mass detection and segmentation based on pseudo-color mammograms and Faster R-CNN.

Table 2 Comparison of our network with traditional ones

Name	Size (MB)	Parameters	Time per image (ms)	AUC	DB
Faster-RCNN	527	1.41e + 08	2.6	0.95	INbreast
DCNN [31]	230	2.5e + 07	6	0.91	DREAM
LSTM [32]	170	1.5e + 04	–	0.93	CIFAR-10
CNN [33]	485	1e + 00.3	4	0.85	OMI-DB

The findings of the competition have proved to be one of the best methods to classification of mammograms for cancer. The DM problem concentrated on recognizing malignant lesions and the picture classification as a whole was the only method that used to get away from the identification mission. We think an injury sensor is much more useful clinically than an arbitrary classification. Just one single marker may be given for a case or breast, but the cancer that is necessary for additional diagnosis or treatment is unable to be identified.

Education approaches have tremendous potential. Our approach can lead to the development of superior CAD systems which increase benefit and reduce the harmful effects of mammography screening and can be used with low ROI imagery.

References

1. Ferlay J, Hery C, Autier P, Sankaranarayanan R (2010) Global burden of breast cancer. In: Breast cancer epidemiology. Springer, pp 1–19
2. Broeders M et al (2012) The impact of mammographic screening on breast cancer mortality in Europe: a review of observational studies. J Med Screen 19:14–25
3. Ponti A, et al (2017) Cancer screening in the European Union. Final report on the implementation of the council recommendation on cancer screening
4. Bae MS et al (2014) Breast cancer detected with screening us: reasons for nondetection at mammography. Radiology 270:369–377
5. Hoff SR et al (2012) Breast cancer: missed interval and screening-detected cancer at full-field digital mammography and screen-film mammography—results from a retrospective review. Radiology 264:378–386
6. American Cancer Society (2018) How Common Is Breast Cancer? https://www.cancer.org/cancer/breast-cancer/about/how-common-is-breast-cancer.html. Accessed 18 Dec 2018
7. Kevin Oeffinger C et al (2015) Breast cancer screening for women at average risk: 2015 guideline update from the American Cancer Society. JAMA 314(15):1599–1614. https://doi.org/10.1001/jama.2015.12783 (**ISSN: 0098-7484**)
8. Breast Cancer Surveillance Consortium (2009) Performance Measures for 1,838,372 Screening Mammography Examinations from 2004 to 2008 by Age—Based on BCSC Data through 2009. http://www.bcsc-research.org/statistics/performance/screening/2009/perf_age.html. Accessed 18 Dec 2018
9. Elter M, Horsch A (2009) CADx of mammographic masses and clustered microcalcifications: a review. Med Phys 36(6Part1 2009):2052–2068. https://doi.org/10.1118/1.3121511 (**ISSN: 2473-4209**)
10. Lehman CD et al (2015) Diagnostic accuracy of digital screening mammography with and without computer-aided detection. JAMA Intern Med 175(11):1828–1837
11. LeCun Y, Bengio Y, Hinton G (2015) Deep learning. Nature 521(7553):436–444. https://doi.org/10.1038/nature14539
12. Aboutalib SS et al (2018) Deep learning to distinguish recalled but benign mammography images in breast cancer screening. Clin Cancer Res. https://doi.org/10.1158/1078-0432.CCR-18-1115 (**ISSN: 1078-0432**)
13. Girshick R (2015) "Fast R-Cnn". In: Proceedings of the IEEE international conference on computer vision, pp 1440–1448. http://www.cv-foundation.org/openaccess/content_iccv_2015/html/Girshick_Fast_R-CNN_ICCV_2015_paper.html (visited on 11/09/2016)
14. Ribli D et al (2017) Detecting and classifying lesions in mammograms with deep learning. In: (2017). arXiv: 1707.08401. http://arxiv.org/abs/1707.08401 (visited on 12/12/2017).
15. Moreira IC et al (2012) INbreast: toward a full-field digital mammographic database. Acad Radiol 19(2):236–248. https://doi.org/10.1016/j.acra.2011.09.014 (**ISSN: 1076-6332**)
16. Hinton GE, Osindero S, Teh Y-W (2006) A fast learning algorithm for deep belief nets. Neural Comput 18(7):1527–1554. https://doi.org/10.1162/neco.2006.18.7.1527 (**ISSN: 0899-7667**)
17. Russakovsky O et al (2015) ImageNet large scale visual recognition challenge. Int J Comput Vision 115(3):211–252. https://doi.org/10.1007/s11263-015-0816-y (**ISSN: 0920-5691**)
18. Ren S, He K, Girshick R, Sun J (2015) Faster R-CNN: towards real-time object detection with region proposal networks. In: Advances in neural information processing systems, pp 91–99
19. Girshick R, Donahue J, Darrell T, Malik J (2016) Region-based convolutional networks for accurate object detection and segmentation. IEEE Trans Pattern Anal Mach Intell 38:142–158. https://doi.org/10.1109/TPAMI.2015.2437384
20. Ren S, He K, Girshick R, Sun J (2015) Faster R-CNN: towards real-time object detection with region proposal networks. Int Conf Neural Inform Process Syst. https://doi.org/10.1109/TPAMI.2016.2577031
21. Girshick R (2015) Fast R-CNN. Comput Sci. https://doi.org/10.1109/ICCV.2015.169
22. Hou HS, Andrews H (1978) Cubic splines for image interpolation and digital filtering. IEEE Trans Acoust Speech Signal Process 26:508–517. https://doi.org/10.1109/TASSP.1978.1163154
23. Zhou C, Chan HP, Paramagul C, Roubidoux MA, Sahiner B, Hadjiiski LM, Petrick N (2004) Computerized nipple identification for multiple image analysis in computer-aided diagnosis. Med Phys 31:2871–2882. https://doi.org/10.1118/1.1800713
24. Wu YT, Zhou C, Chan HP, Paramagul C, Hadjiiski LM, Daly CP, Douglas JA, Zhang YH, Sahiner B, Shi JZ, Wei J (2010) Dynamic multiple thresholding breast boundary detection algorithm for mammograms. Med Phys 37:391–401. https://doi.org/10.1118/1.3273062
25. Kus P, Karagoz I (2012) Fully automated gradient based breast boundary detection for digitized X-ray mammograms. Comput Biol Med 42:75–82. https://doi.org/10.1016/j.compbiomed.2011.10.011
26. Krizhevsky A, Sutskever I, Hinton GE (2012) ImageNet classification with deep convolutional neural networks. Int Conf Neural Inform Process Syst. https://doi.org/10.1145/3065386
27. Ren S, He K, Girshick R, Sun J (2015) Faster R-CNN: towards real-time object detection with region proposal networks. Int Conf Neural Inform Process Syst. https://doi.org/10.1109/TPAMI.2016.2577031
28. Samuelson FW, Petrick N, Paquerault S (2007) Advantages and examples of resampling for CAD evaluation. In: IEEE international symposium on biomedical imaging: from nano to macro, pp 492–495. https://doi.org/10.1109/ISBI.2007.356896
29. Bornefalk H, Hermansson AB (2005) On the comparison of FROC curves in mammography CAD systems. Med Phys 32:412–417. https://doi.org/10.1118/1.1844433
30. Fotin SV, Yin Y, Haldankar H, Periaswamy S (2016) Detection of soft tissue densities from digital breast tomosynthesis: comparison of conventional and deep learning approaches. Comput Aided Diagn Med Imaging. https://doi.org/10.1117/12.2217045
31. Gao F, Wu T, Li J, Zheng B, Ruan L, Shang D, Patel B (2018) SD-CNN: a shallow-deep CNN for improved breast cancer diagnosis. Comput Med Imaging Graph 70:53–62

32. Budak Ü, Cömert Z, Rashid ZN, Şengür A, Çıbuk M (2019) Computer-aided diagnosis system combining FCN and Bi-LSTM model for efficient breast cancer detection from histopathological images. Appl Soft Comput 85:105765
33. Agarwal R, Diaz O, Yap MH, Lladó X, Martí R (2020) Deep learning for mass detection in Full Field Digital Mammograms. Comput Biol Med 121:103774